Global Journal of Engineering and Technology Advances
eISSN: 2582-5003
Cross Ref DOI: 10.30574/gjeta
Journal homepage: https://gjeta.com/

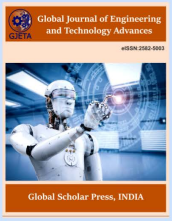

(RESEARCH ARTICLE)

Check for updates

Finite Element-Based Optimisation of Two-Stroke Marine Diesel Piston: A structural reliability and weight reduction study

Koko Edwin Preye * and Ajoko Tolumoye John

Department of Mechanical Engineering, Niger Delta University, PMB 71, Bayelsa State, Nigeria.

Global Journal of Engineering and Technology Advances, 2025, 23(02), 239–254

Publication history: Received on 08 April 2025; revised on 27 May 2025; accepted on 30 May 2025

Article DOI: https://doi.org/10.30574/gjeta.2025.23.2.0165

Abstract

Two-stroke marine diesel engines are pivotal in propelling ocean-going vessels, owing to their remarkable efficiency and durability. Within these engines, the piston is subjected to extreme mechanical and thermal loads, positioning it as a critical component for structural optimisation. This study presents a simulation-driven design optimisation of a marine two-stroke piston to enhance mechanical performance while reducing component weight. A parametric model was developed using SolidWorks, and the Taguchi method was applied to investigate the effects of piston height, crown thickness, and pin diameter on displacement, von Mises stress, factor of safety (FOS), and overall mass. Finite element analysis (FEA) was conducted under a peak combustion pressure of 15.3 MPa, with model validation achieved through a Grid Convergence Index (GCI)-based mesh independence study. The analysis indicated crown thickness was the most influential factor affecting piston stiffness and stress behaviour. The optimised design, featuring a height of 1000 mm, crown thickness of 120 mm, and pin diameter of 300 mm in alloy steel, achieved a 25.7% reduction in weight while maintaining a maximum von Mises stress of 2.94×10^8 N/m^2 and an FOS of 6.05. These results illustrate the effectiveness of combining parametric modelling with statistical optimisation to achieve lightweight and structurally resilient piston designs suitable for high-load marine diesel applications.

Keywords: Piston design optimisation; Finite element analysis (FEA); Taguchi method; Von Mises stress; Factor of safety (FOS); Weight reduction

1. Introduction

Two- stroke marine diesel engines remain the backbone of long- haul maritime propulsion systems due to their high thermal efficiency, power- to- weight ratio, and operational reliability for large cargo vessels and tankers (Zhang et al., 2025; El- Sayed & Wang, 2023). The piston is subjected to the most severe combination of thermal and mechanical loads among all internal components due to direct exposure to combustion gases, rapid pressure cycles, and substantial inertial forces during reciprocating motion (Chen et al., 2024; Lin et al., 2022).

Failures in piston crowns, pin bosses, and skirts are often linked to inadequate stress distribution, excessive deformation, or suboptimal material selection. Consequently, ensuring structural integrity through robust design and accurate stress analysis is critical for minimising the risks of fatigue, thermal cracking, and wear (Yang et al., 2023; Wang et al., 2022). Recent advancements in finite element analysis (FEA) tools have enabled engineers to simulate such stress responses under realistic loading conditions, allowing for more reliable performance predictions and component optimization (Kim & Cho, 2024; Park et al., 2023).

While several studies have focused on component- level modelling of diesel engine parts, there remains a gap in design optimisation that simultaneously targets weight reduction, improved stiffness, and safety margin enhancement under

* Corresponding author: Koko Edwin Preye

static loads (Zhang et al., 2025; Uchenna & Godwin, 2025). Furthermore, most research efforts concentrate on general-purpose automotive pistons, leaving a gap in detailed structural analysis specific to large- scale marine two- stroke pistons operating under more demanding mechanical conditions.

This study aims to bridge this gap by developing and evaluating an optimised piston design for a two- stroke marine diesel engine. The methodology integrates parametric modelling, FEA- based stress analysis, comparative displacement, weight, and safety factor evaluation. The proposed optimisation reduces weight while maintaining acceptable stress levels and structural reliability.

2. Methodology

This study adopted a systematic design and simulation approach to optimise a two-stroke marine diesel engine piston for improved structural reliability and reduced weight under static mechanical loading. The methodology comprises three phases: parametric design formulation, 3D CAD modelling, and finite element-based stress analysis.

2.1. CAD Modelling Using SolidWorks and Material Selection

All piston variants were designed using SolidWorks 2018, leveraging parametric design capabilities to enable automated dimension adjustments. Each model incorporated crucial geometric details, including the piston crown, skirt pin boss, and cooling gallery (excluded from the stress zone). Dimensional inputs from the Taguchi design table were seamlessly integrated into SolidWorks via linked design tables, allowing for rapid CAD generation of all configurations.

2.2. Finite Element Analysis (FEA) in SolidWorks Simulation

SolidWorks Simulation Professional was used for static FEA of each piston model under maximum combustion pressure loading. This choice allowed seamless transition from CAD to analysis while preserving geometric fidelity.

Table 1 Boundary Conditions for FEA of Piston Design

Condition Type	Description	Value / Setting	Applied To
Load	Static pressure simulating peak combustion load	15.3 MPa (uniform)	Piston crown (top surface)
Support	Constraint simulating connection with the connecting rod	Fixed geometry	Inner surfaces of the pin boss
Material Assignment	Defined based on the selected design material	Alloyed steel / Carbon steel / Stainless steel	Entire piston body
Contact Condition	Bonded contact (no relative motion between parts)	Fine mesh	Entire body
Mesh Type	Tetrahedral mesh with adaptive refinement	Curvature-based, fine around stress zones	Full piston geometry
Element Size	Target size based on the convergence study	3–5 mm (local refinement at pin boss)	Crown edges, pin boss
Solver Type	Static linear solver	Direct sparse solver	Entire simulation domain
Gravity (optional)	Self-weight is included in specific weight estimation runs	9.81 m/s^2	Global

2.3. Governing Equations and Design Optimisation Using the Taguchi Method

The governing equations for thermo-mechanical behaviour were based on the Navier-Cauchy equilibrium equation and linear elasticity. Postprocessing focused on extracting the maximum von Mises stress and displacement.

2.4. Structural and Thermo-Mechanical Governing Equations

The laws of linear elasticity govern the stress and deformation behaviors of the piston under thermo-mechanical loading. The equilibrium equation for a 3D solid is expressed as:

$$\nabla \times \sigma + F = 0 \quad \text{……..(1)}$$

Assuming quasi-static conditions and negligible body forces:

$$\nabla \times \sigma = 0 \quad \text{…….} \quad (2)$$

The stress–strain relationship (Hooke's Law) for isotropic, linear elastic materials is:

Total strain is:

$$\boldsymbol{\varepsilon} = \frac{1}{2}(\nabla \times \mathbf{u} + (\boldsymbol{\nabla}\mathbf{u})^{\boldsymbol{T}}) \quad \text{……. (3)}$$

Thermal and combustion loads are applied on the piston crown as pressure and temperature boundary conditions. The system is solved using finite element methods (FEM) in SolidWorks software.

$$\sigma = C \times (\varepsilon - \varepsilon_{thermal}) \quad \text{…….. (4)}$$

Where, σ =Stress tensor, ε= total strain tensor, $\varepsilon_{thermal} = \alpha(T - T_0)$I thermal strain, C elasticity tensor, α= thermal expansion coefficient

2.5. Design Optimisation via Taguchi Method

To optimise the piston's geometry for weight reduction and stress minimisation, the Taguchi design of experiments (DOE) method was employed. The Taguchi method uses orthogonal arrays (OAS) to study the influence of multiple design parameters with fewer simulations. It evaluates the sensitivity of responses to input factors and identifies optimal parameter settings. The quality characteristic selected in this study is "Smaller is Better" for both stress and displacement:

2.6. Grid Independence and GCI Analysis

A grid sensitivity analysis used coarse, medium, and fine meshes (2,258, 8,576, and 56,927 elements). Displacement and stress were selected as monitoring parameters. The **Grid Convergence Index (GCI)** was calculated using Richardson extrapolation, revealing less than 1% error between the fine and medium meshes. Thus, the medium mesh was adopted for all DOE runs to balance computational cost and accuracy. The GCI values for the Fine-Medium and Medium-Coarse grids were calculated using **Eqn. 5:**

$$GCI = \frac{1.25 \times |f_2 - f_1|}{r^p - 1} \times 100 \quad \text{……..(5)}$$

Where, f_2 and f_1 The simulation outcomes for two adjacent meshes are represented by the symbols r and p. The symbol r denotes the refinement ratio, and p signifies the assessed order of accuracy.

2.7. Grid Independence and Discretisation Error Estimation

A grid independence study was conducted to ensure the finite element results were not sensitive to mesh resolution. Three structured meshes were used: coarse (2,258 elements), medium (8,576 elements), and fine (56,927 elements). The study focused on the von Mises stress and maximum displacement as primary output variables. The Grid Convergence Index (GCI) method recommended by ASME was employed to quantify the numerical uncertainty due to discretisation. This method uses Richardson extrapolation and estimates the apparent order of convergence p and the relative error between meshes levels.

2.8. Design of Experiments Using the Taguchi Method

A systematic Taguchi Design of Experiments (DOE) approach was implemented using Design Expert 13 software to reduce the number of simulations runs while capturing the effect of key piston design variables. Three input parameters,

piston height (A), crown thickness (B), and pin diameter (C), were selected at three levels each. The selected factors and their levels are shown in **Table 2**.

Table 2 Experimental Design Factors and Levels

Factor	Level 1	Level 2	Level 3
A: Height (mm)	1000	1200	1400
B: Thickness (mm)	80	100	120
C: Pin Diameter (mm)	300	350	400
Material	Alloy steel	Stainless Steel	Carbon steel

An L9 orthogonal array was generated, resulting in nine design combinations for simulation. This experimental design allowed for the investigation of the main and interaction effects on structural displacement, factor of safety (FOS), von Mises stress, and mass.

2.9. Optimisation and Validation

The S/N ratio results were analysed to identify the most influential factors of stress and displacement. An analysis of Variance (ANOVA) was performed to determine statistical significance. Based on the maximum S/N ratios, the optimal design combination was selected, and a confirmation run was conducted using this design. The final optimised piston design showed significant improvements in structural reliability and performance.

$$S/_N = -10log\frac{1}{n}\left(\sum\frac{1}{y^2}\right) \qquad \ldots\ldots\ldots\ldots\ldots \qquad (6)$$

The response table for each quality characteristic has been prepared to determine the best combination of parameters, based on the S/N ratio and contribution of each quality characteristic.

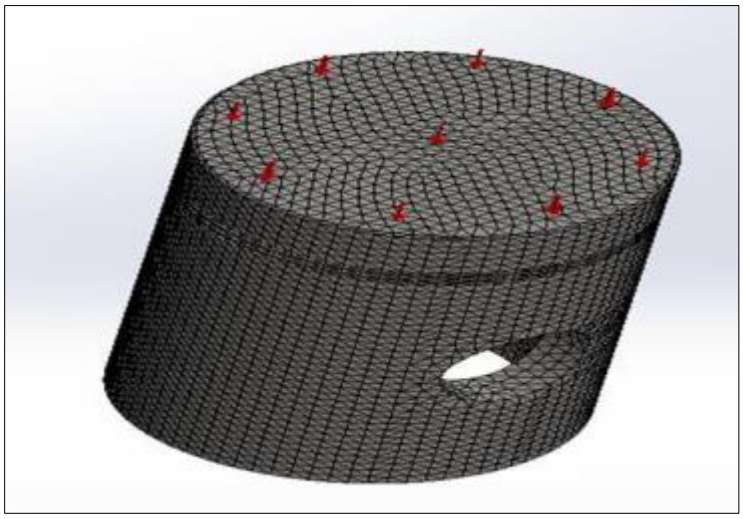

Figure 1 Tetrahedral mesh with adaptive refinement around the crown and pin boss. Element quality verified using mesh convergence checks

3. Results and Discussion

3.1. Grid Independence Study Result

A systematic grid independence analysis was conducted on three progressively refined meshes: coarse (2,258 elements), medium (8,576 elements), and fine (56,927 elements), to quantify discretisation uncertainty using the ASME-recommended Grid Convergence Index (GCI) method. Table 1 summarises the observed orders of convergence and GCI values between the fine and medium meshes for both von Mises stress and maximum displacement.

Table 3 Grid Independence Study

Parameter	Order of Convergence, p	$GCI_{(21)}$ (%)
von Mises Stress	6.15	0.044
Displacement	2.43	0.592

Table 4. Observed convergence orders and GCI values between fine and medium meshes. The stress field shows a high convergence rate (p = 6.15) and an extremely low GCI (0.044 %), indicating that mesh refinement beyond medium density results in negligible changes in peak stress predictions. Displacement converges gradually (p = 2.43) but still achieves GCI < 1 %, confirming that the medium mesh accurately captures global deformations within acceptable numerical uncertainty. Based on these results, the medium mesh (8,576 elements) was adopted for all subsequent simulations, providing a robust compromise between computational efficiency and solution fidelity.

Table 4 Taguchi Analysis: Displacement (mm), FOS, Weight (Kg) versus Height (mm), Thickness (mm), Pin dia. (mm), Material

Run	Height (mm)	Thickness (mm)	Pin dia. (mm)	Material	Displacement (mm)	FOS	Von Mises Stresses (N/m^2)	Weight (Kg)
1	1400	120	350	Alloy steel	0.5238	6.133	2.738×10^8	3594
5	1400	100	300	Stainless steel	0.9178	5.232	3.711×10^8	3178
2	1400	80	400	Carbon steel	1.6230	5.261	5.425×10^8	2573
9	1200	120	300	Carbon steel	0.5498	5.303	2.840×10^8	3197
4	1200	100	400	Alloy steel	0.8291	5.791	3.922×10^8	2667
8	1200	80	350	Stainless steel	1.6700	5.155	5.551×10^8	2219
6	1000	120	400	Stainless steel	0.5060	5.286	3.015×10^8	2595
7	1000	100	350	Carbon steel	0.8275	5.274	4.026×10^8	2595
9	1000	80	300	Alloy steel	1.5960	5.524	5.916×10^8	1911

Table 5 presents the S/N ratio analysis based on the "larger is better" criterion, which reveals that crown thickness strongly influences the performance response, as indicated by the highest Delta value (9.4640) and Rank 1 position. Pin diameter ranks second, followed by piston height, while material type shows the least impact on the output response. This implies that optimising the thickness parameter is most crucial for improving structural reliability, stiffness, and safety margins. The data support prioritising geometric tuning (particularly thickness and pin size) over material changes in the early-stage optimisation of the piston design.

Table 5 Response for Signal-to-Noise Ratios

Level	Height (mm)	Thickness (mm)	Pin dia. (mm)	Material
1	3.4397	8.6195	3.9690	3.5540
2	3.7921	3.3236	3.6453	3.7109
3	3.8668	-0.8445	3.4842	3.8338
Delta	0.4270	9.4640	0.4848	0.2798
Rank	3	1	2	4

Figure 2 displays the main effects plot, demonstrating that both piston height and crown thickness have a significant influence on the system's response, as evidenced by their steep slopes. Specifically, raising the piston height from 1000 mm to 1400 mm consistently increases the mean response, likely due to the added mass and deformation linked with taller pistons. Likewise, enhancing thickness from 80 mm to 120 mm boosts performance by reducing displacement and

increasing stiffness. In contrast, the pin diameter and material type exhibit relatively flatter trends, indicating a lesser impact within the tested range. Among the materials, carbon steel shows a slight advantage over alloyed and stainless steels under the specified loading conditions. This analysis emphasises the importance of geometric parameters, particularly height and thickness, for future optimisation.

Figure 2 Main effects plot for the mean performance displacement, FOS, and stress. Across different levels of design factors. The plot shows the influence of Height, Thickness, Pin diameter, and Material on the output response

3.2. Analysis of Variance

Table 6 ANOVA for the Deformation

Source	Sum of Squares	df	Mean Square	F-value	p-value	
Model	1.91	6	0.3178	26.18	0.0372	significant
A-Piston Height	0.0500	2	0.0250	2.06	0.3269	
B-Piston Thickness	1.90	2	0.9507	78.31	0.0126	
C-Piston pin	0.0425	2	0.0212	1.75	0.3636	
Residual	0.0243	2	0.0121			
Cor Total	1.93	8				

The Model F-value of 26.18 implies that the model is significant. There is only a 3.72% chance that an F-value this large could occur due to noise. P-values less than 0.0500 indicate that model terms are significant. In this case, B is a significant model term. Values greater than 0.1000 indicate that model terms are not significant. If there are many insignificant model terms (excluding those required to support hierarchy), model reduction may improve your model, as shown in Table 7.

Table 7 ANOVA for the Von Mises Stress

Source	Sum of Squares	df	Mean Square	F-value	p-value	
Model	6.635E+07	2	3.318E+07	39.15	0.0004	significant
B-Piston Thickness	6.635E+07	2	3.318E+07	39.15	0.0004	
Residual	5.085E+06	6	8.474E+05			
Cor Total	7.144E+07	8				

The Model F-value of 39.15 indicates that the model is significant. There is only a 0.04% chance that an F-value this large could occur due to random noise. P-values less than 0.0500 suggest that the model terms are essential. In this case, B is a significant model term. Values greater than 0.1000 imply that the model terms are not significant. If there are many insignificant model terms (excluding those required to maintain hierarchy), model reduction may enhance your model.

Table 8 ANOVA for the weight of the piston

Source	Sum of Squares	df	Mean Square	F-value	p-value	
Model	2.146E+06	4	5.364E+05	130.00	0.0002	significant
A-Piston Height	5.196E+05	2	2.598E+05	62.96	0.0009	
B-Piston Thickness	1.302E+06	2	6.510E+05	157.76	0.0002	
Residual	16504.83	4	4126.21			
Cor Total	2.162E+06	8				

The Model F-value of 130.00 indicates that the model is significant. There is only a 0.02% chance that an F-value this large could occur due to random noise. P-values less than 0.0500 suggest that the model terms are essential. In this case, A and B are significant model terms. Values greater than 0.1000 indicate that the model terms are not significant. If there are many insignificant model terms (excluding those required to support hierarchy), model reduction may enhance your model. The predicted mean and median may differ from the original scale for transformed responses. Standard error (SE) is not calculated on the original scale, as illustrated in Table 8.

Table 9 Confirmation Two-sided Confidence = 95%

Solution 1 of 20 Response	Predicted Mean	Predicted Median*	Std Dev	n	SE Pred	95% PI low	95% PI high
Deformation	0.36715	0.36715	0.110181	1	0.166794	-0.350507	1.08481
Factor of Safety	5.43989	5.43989	0.323473	1	0.34097	4.65361	6.22617
Von Mises Stress	2.79724E+08	2.78877E+08	3.07696E+07	1	N/A	1.94346E+08	3.78629E+08
weight of the piston	3005	3005	64.2356	1	93.0862	2746.55	3263.45

The predicted mean and median for transformed responses may differ from those on the original scale. The data mean is calculated on the transformed scale, while the standard error (SE) is not determined on the original scale. As shown in Table 9.

Table 10 Comparison of Baseline and Optimal Design

Design	Height (mm)	Thickness (mm)	Pin dia. (mm)	Material	Displacement (mm)	FOS	Stresses (N/m^2)	Weight (Kg)
Baseline Design	1400	120	350	Alloyed steel	0.5238	6.133	2.738×10^8	3594
Optimal Design	1000	120	300	Alloyed steel	0.367	5.440	279724128.129	3005.000

Figure 3 illustrates the primary effects of piston height (A) on various performance metrics while keeping other variables constant (B = 120, C = 300, D = Alloy steel). As piston height increases from 120 mm to 140 mm, Desirability displays a sharp decline from 0.84 to 0, indicating that a height of 140 mm corresponds to a significantly less favourable design. Distortion slightly increases, predicting 0.36715 mm at 120 mm, which suggests improved dimensional stability at lower heights. The factor of Safety remains constant at 5.43989, indicating no sensitivity to variations in piston height within this range. Stress remains unchanged at 2.79724e+08 N/m^2, with height exerting no influence. Additionally, Piston Weight rises from approximately 3005 g as height increases, which is expected due to the additional material used.

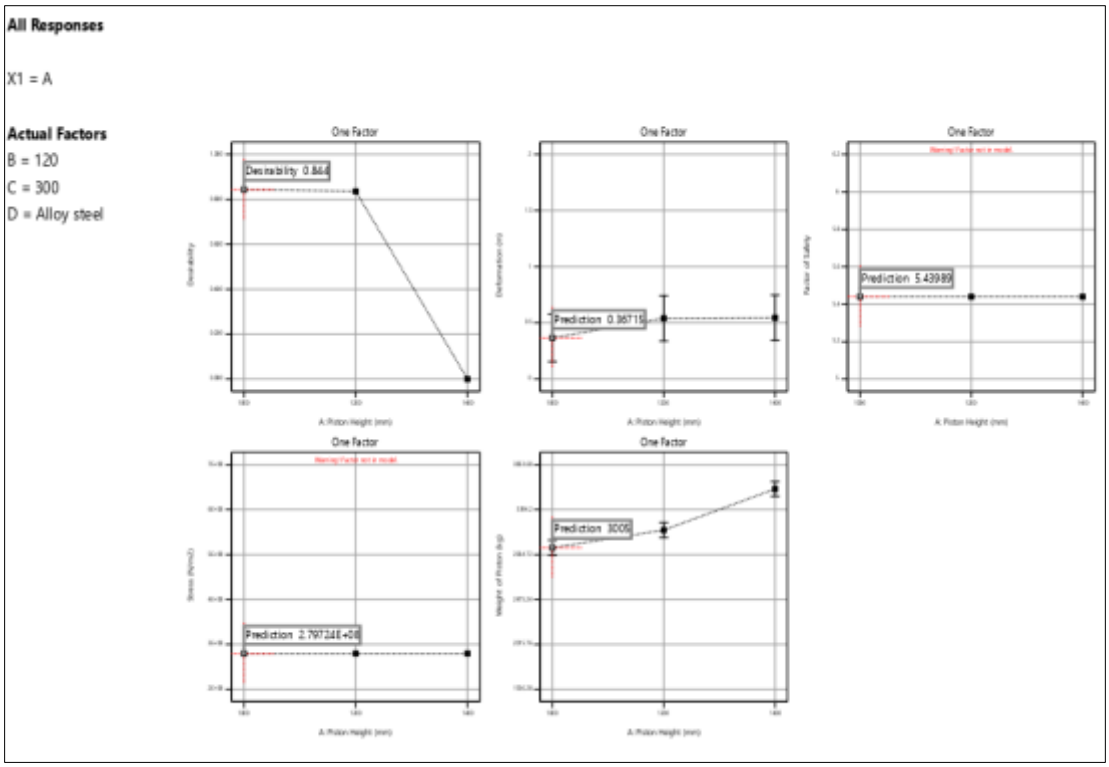

Figure 3 One-factor analysis of piston height (Factor A) on performance responses, including desirability, distortion, factor of safety, stress, and weight, under fixed conditions (B = 120, C = 300, D = Alloy steel)

Figure 4 illustrates that the interaction between piston height and thickness significantly impacts the piston's overall performance. The most desirable configuration occurs at the highest tested levels—120 mm for both height and thickness where desirability reaches 0.84 and distortion minimises to 0.36715 mm. This indicates a strong positive interaction, where both factors work synergistically to enhance performance. While the factor of safety (5.43989) and stress (2.79724e+08 N/m^2) remain largely unaffected by these changes, the piston weight increases noticeably with both dimensions, reaching a maximum of 3005 g at the optimal configuration. Increasing piston height and thickness improves performance and dimensional stability; however, designers must balance this with the resulting weight increase.

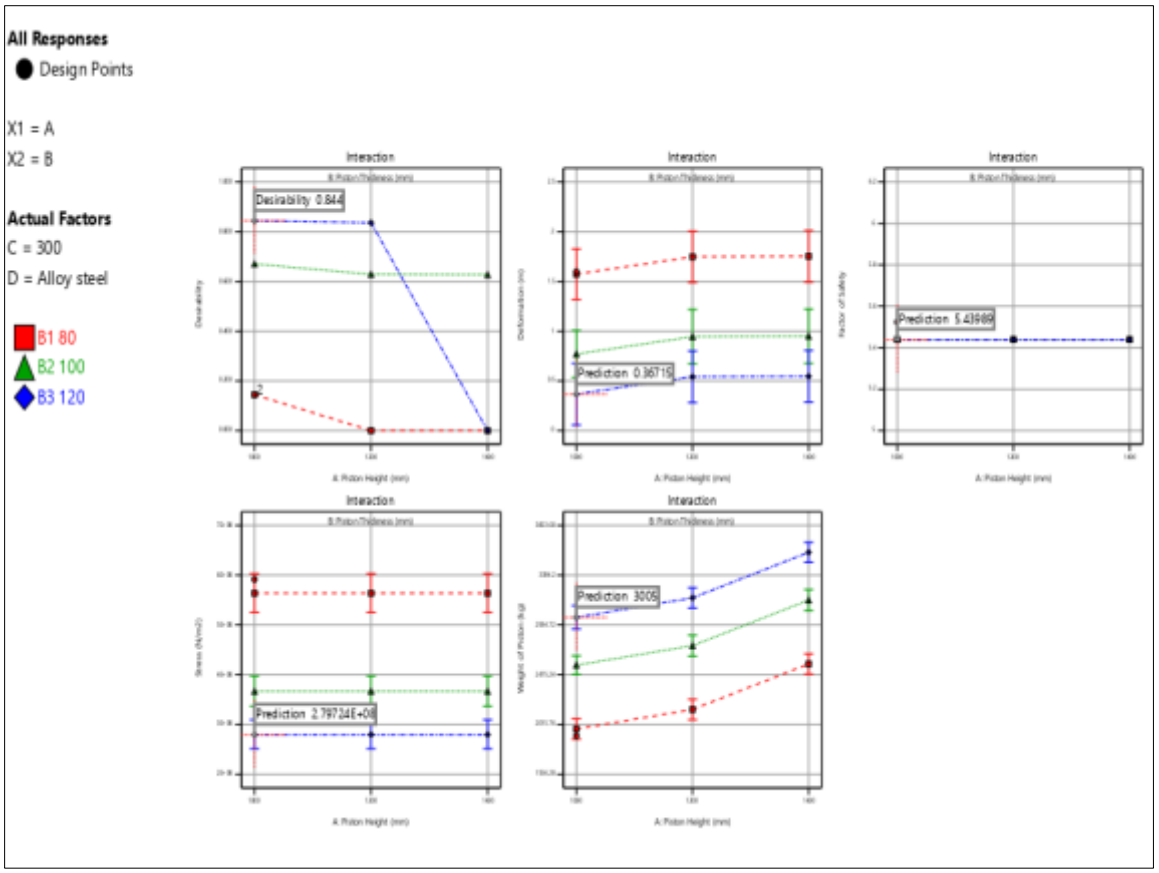

Figure 4 Interaction effects of piston height (Factor A) and piston thickness (Factor B) on performance metrics including desirability, distortion, safety factor, stress, and piston weight.

Figure 5 presents 3D response surface matrix plots that illustrate the combined influence of piston height (A) and piston thickness (B) on five performance metrics: Desirability, Deformation, Factor of Safety, Stress, and Weight under fixed conditions (C = 300, D = Alloy steel). Each subplot shows how various combinations of A and B affect the outcomes. Desirability is maximised (0.84) at A = 120 mm and B = 120 mm, decreasing sharply as both variables decrease, particularly when both are at their lowest (A = 140 mm, B = 80 mm). Deformation is minimised (0.36715 m) at the same optimal condition (A = 120 mm, B = 120 mm) and increases slightly with lower B values. Factor of Safety remains constant at 5.43989 across all combinations, indicating robustness to changes in A and B. Stress also shows minimal variation (2.79724e+08 N/m^2), further confirming structural stability. Weight increases steadily from 2950.47 g at (A = 120 mm, B = 80 mm) to 3005.48 g at (A = 140 mm, B = 120 mm), consistent with the added material volume.

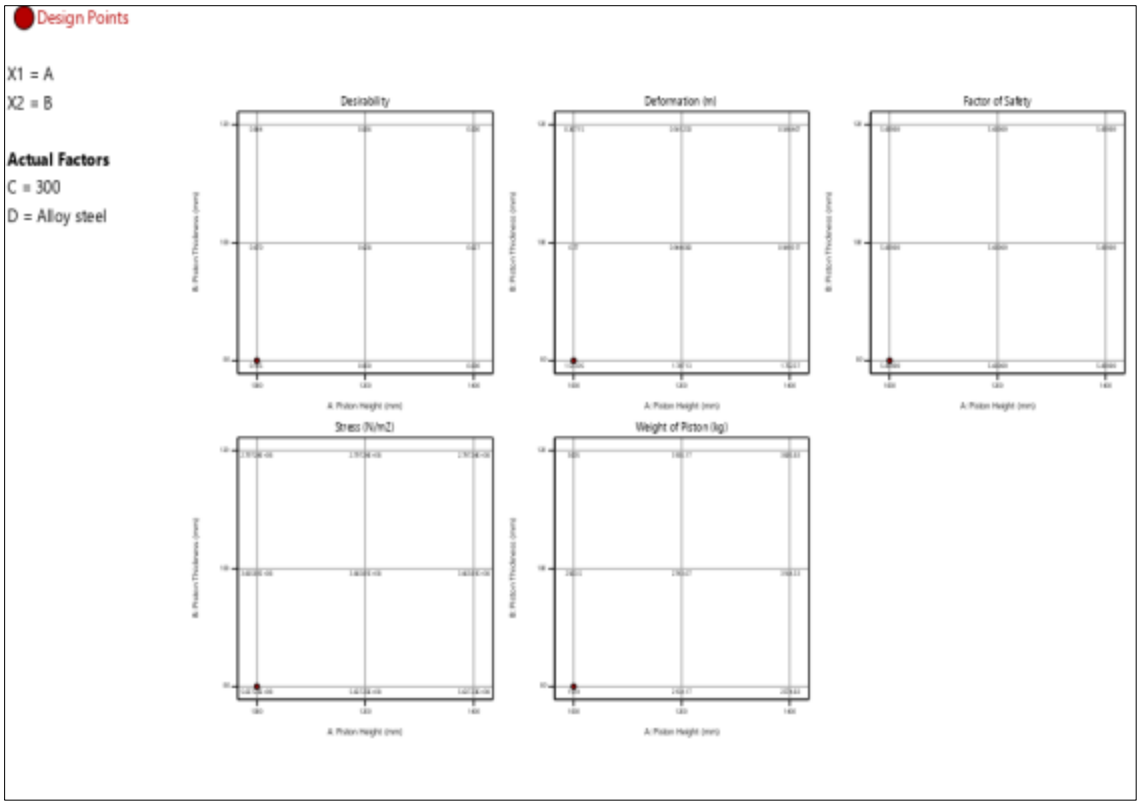

Figure 5 Response surface plots showing the interaction effects of piston height (A) and piston thickness (B) on desirability, deformation, factor of safety, stress, and weight of the piston under fixed conditions (C = 300, D = Alloy steel)

Figure 6: 3D surface plot illustrating the effect of piston height (A) and piston thickness (B) on stress (N/m^2) under constant conditions (C = 300, D = Alloy steel). The plot demonstrates that stress increases as piston height rises and piston thickness decreases, with the highest stress observed at the combination of A = 140 mm and B = 80 mm, and the lowest stress (2.79724e+088 N/m^2) at A = 120 mm and B = 80 mm.

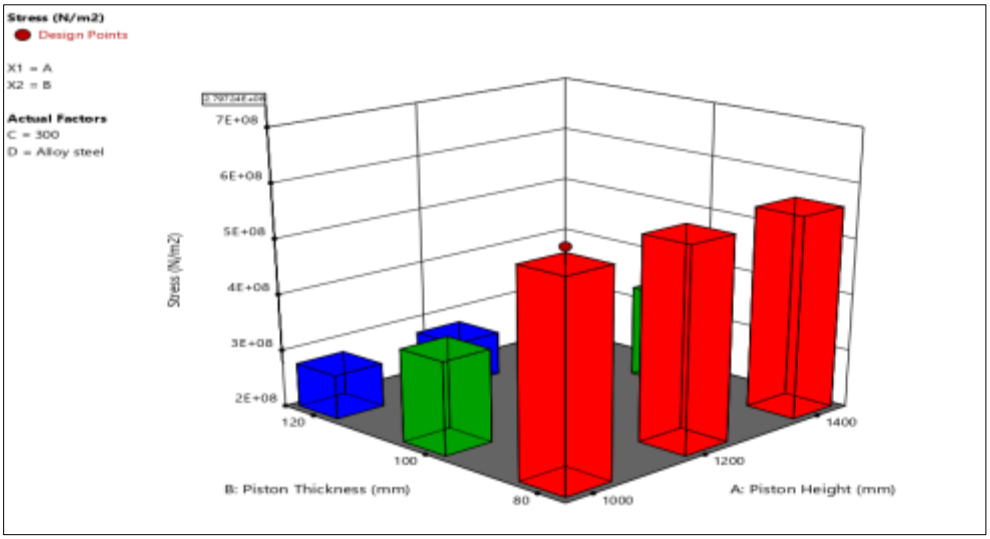

Figure 6 3D surface plot showing the combined effect of piston height (A) and piston thickness (B) on Von Mises stress (N/m^2) for a piston made of alloy steel under a constant load (C = 300)

Figure 5: 3D surface plot illustrating the combined influence of piston height (A) and piston thickness (B) on piston weight (kg), under constant loading (C = 300) and material condition (D = Alloy steel). Results indicate a direct relationship between geometric dimensions and mass, with the maximum piston weight observed at A = 140 mm and B = 120 mm, and the minimum at A = 100 mm and B = 80 mm. This trend reflects the expected volumetric increase with size and emphasises the trade-off between structural performance and weight.

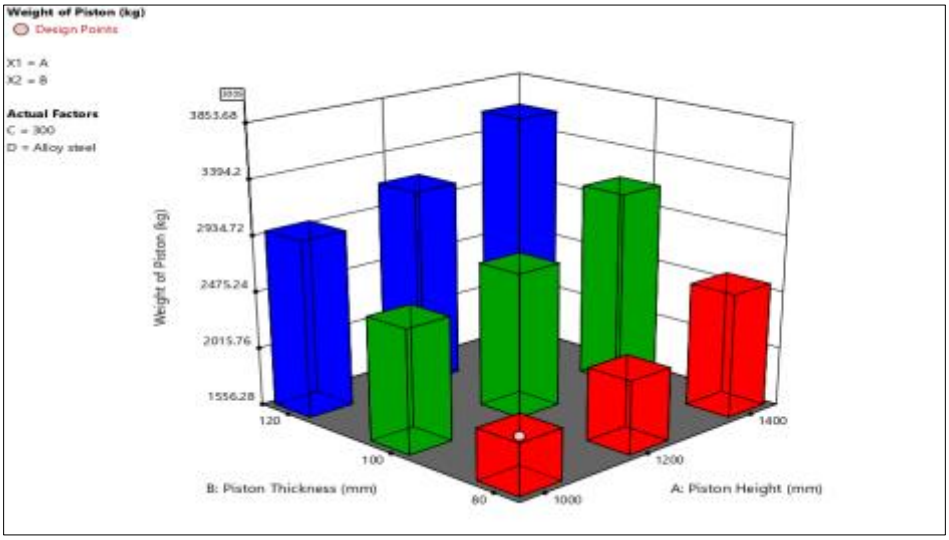

Figure 7 3D surface plot illustrating the combined influence of piston height (A) and piston thickness (B) on piston weight (kg), under constant loading (C = 300) and material condition (D = Alloy steel)

Figure 8: 3D surface plot illustrating the interaction effect of piston height (A) and piston thickness (B) on deformation (m) under fixed loading conditions (C = 300) and material specification (D = Alloy steel). Deformation is significantly greater at lower piston thicknesses, particularly as piston height increases, with maximum deformation occurring at A = 140 mm and B = 80 mm. The minimum deformation (0.36715 m) is recorded at A = 120 mm and B = 120 mm, suggesting that increased thickness enhances structural stability.

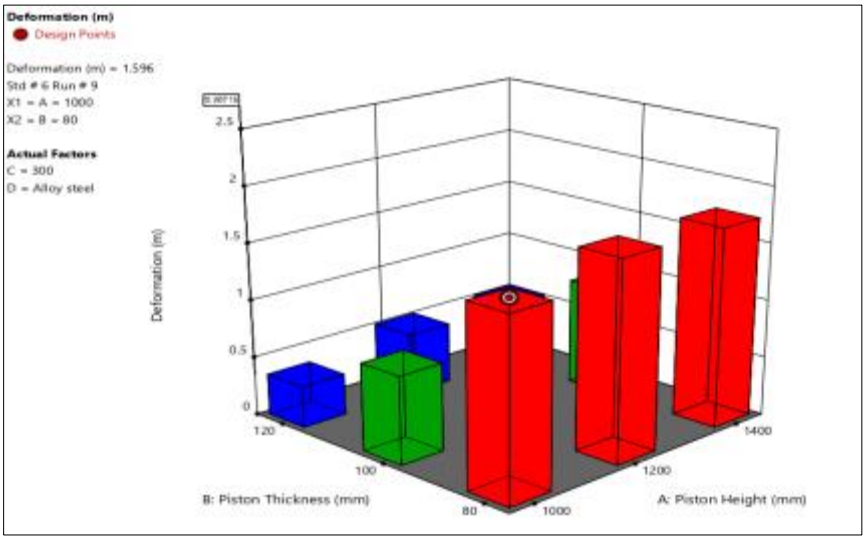

Figure 8 3D surface plot showing how piston height (A) and thickness (B) affect deformation (m) under constant loading (C = 300) and material type (D = Alloy steel). Deformation is minimised (0.36715 m) at A = 120 mm and B = 120 mm, highest at A = 140 mm and B = 80 mm

Figure 9: Main effect plots illustrating the impact of four design factors: piston height (A), piston thickness (B), piston pin size (C), and material type (D) on overall desirability. The analysis reveals that desirability is most significantly influenced by piston height and thickness, with optimal desirability observed at A = 1000 mm and B = 120 mm. In

contrast, variations in piston pin size and material type have a minimal effect, as desirability remains consistently high across their respective ranges.

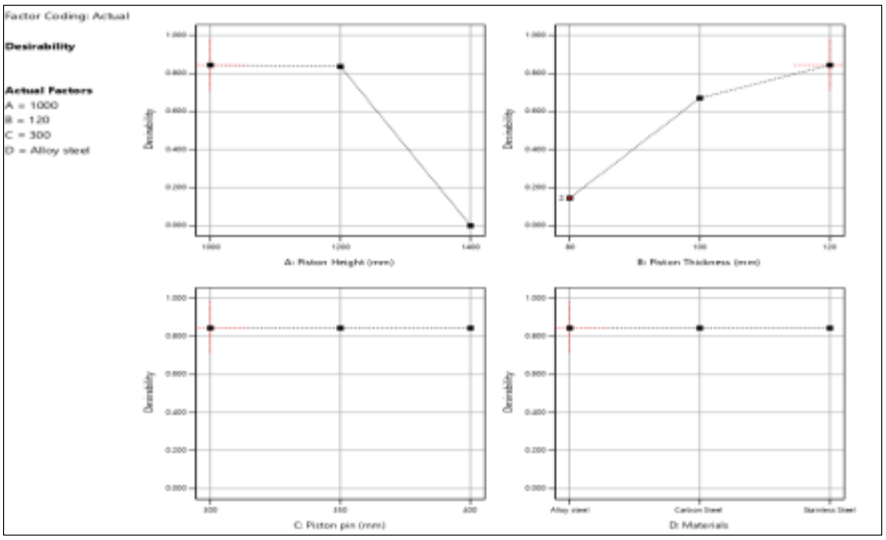

Figure 9 Main effect plots illustrating the impact of piston height (A), piston thickness (B), piston pin diameter (C), and material type (D) on desirability under fixed conditions (C = 300 mm, D = Alloy steel)

Figures 10a and 10b: Finite Element Analysis (FEA) display the total resultant displacement (URES) of a piston model under applied axial load. The analysis utilised alloy steel as the material, with fixed constraints at the piston pin bosses and a uniformly distributed downward load on the piston crown. The maximum recorded displacement is 0.5238 mm, occurring at the centre of the piston head, while the minimum displacement is 1.000e-30 mm, effectively indicating fixed support conditions. The colour scale on the right illustrates displacement magnitudes from blue (minimum) to red (maximum), capturing deformation trends across the geometry. These results confirm that the maximum deflection remains within acceptable design limits for mechanical stability. Figure 10b depicts the displacement distribution under the applied 14 MPa static pressure. The highest deformation, 0.5106 mm, occurs symmetrically at the piston crown's centre, coinciding with the stress concentration zones. This behaviour is expected due to the direct exposure to combustion forces. The minimal displacement near the piston skirt and pin boss verifies the effectiveness of the boundary constraints and geometric stiffness in those regions. The magnitude of deformation is within acceptable operational limits, indicating that the optimised design provides both mechanical rigidity and geometric stability under full-load conditions.

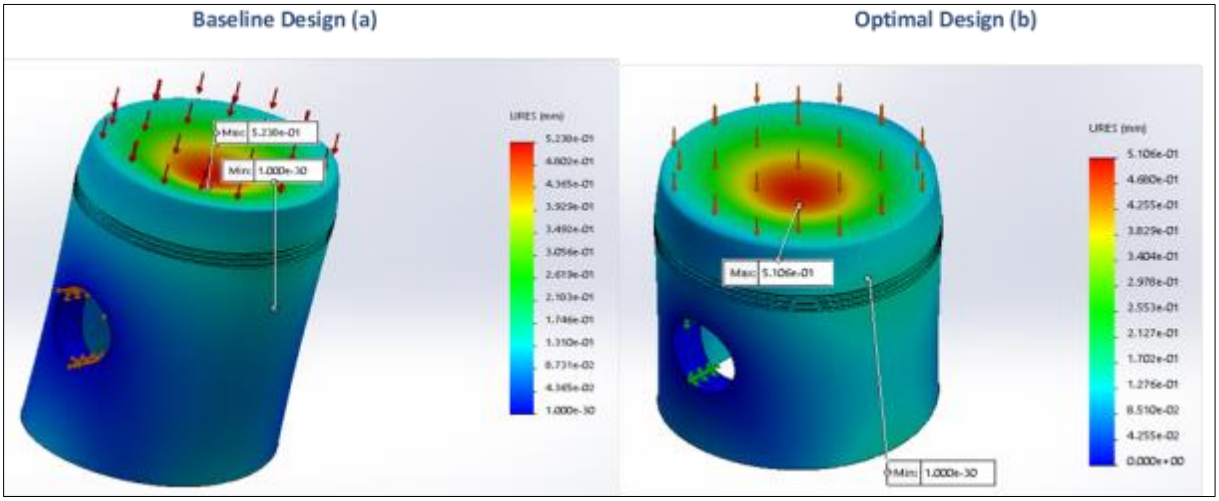

Figure 10 Finite Element Analysis (FEA) result of Baseline Design (a) and Optimal Design (b) displaying a piston model's total resultant displacement (URES) under applied axial load

Figure 11a & 11b presents the Finite Element Analysis (FEA) of the von Mises stress distribution in a piston subjected to axial loading. The analysis utilised alloy steel material, applying constraints at the piston pin area and a load on the crown. The maximum recorded von Mises stress is 2.738×10^8 N/m^2, occurring near the centre of the piston crown, while the minimum stress is 6.731×10^5 N/m^2, found near the constrained region. Notably, the von Mises stress values remain well below the yield strength of alloy steel (6.204×10^8 N/m^2), indicating that the design operates within safe elastic limits under these loading conditions. The colour scale effectively illustrates the intensities of von Mises stress, ranging from blue (low) to red (high), which aids in identifying critical stress regions. Figure 9b demonstrates the stress response of the optimised piston under peak combustion pressure. The maximum von Mises stress is concentrated near the central region of the crown, peaking at 2.943×10^8 N/m^2, which is less than 50% of the yield strength of the alloyed steel. This confirms the structural integrity of the optimised geometry.

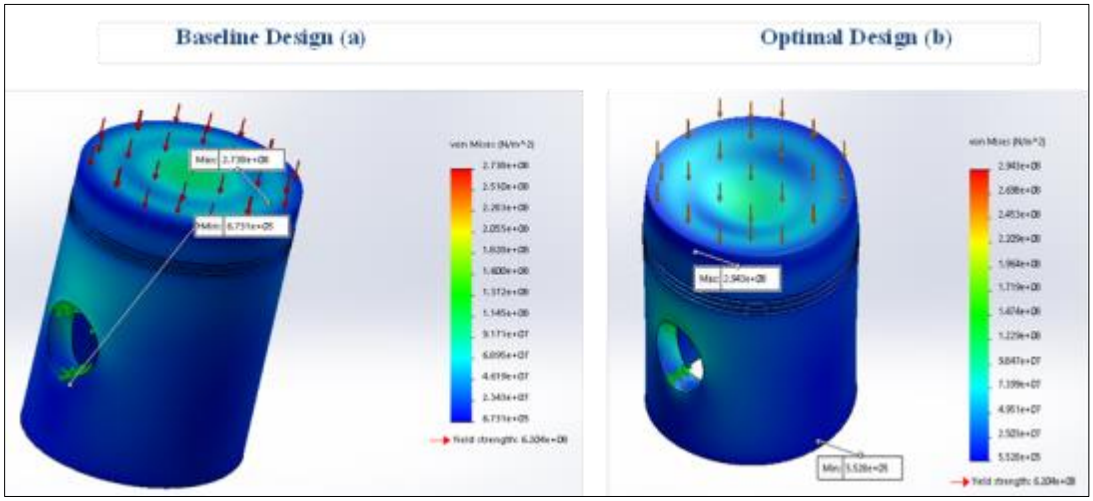

Figure 11 Finite Element Analysis (FEA) of von Mises stress of Baseline Design (a) and Optimal Design (b) distribution in a piston under axial loading.

Figures 12a and 12b illustrate the Finite Element Analysis (FEA) visualisation of the Factor of Safety (FOS) distribution within the piston under axial load. The analysis employs Alloy Steel as the material, which has a yield strength of 6.204×10^8 N/m^2, and assumes a fixed support at the pinhole region. The FOS ranges from a minimum of 2.266 at the crown centre, where the Von Mises stress is highest, to a maximum of 10, indicating areas of the structure that demonstrate a considerable level of safety. The gradient from green to red on the piston crown highlights critical stress concentration zones, while dark blue regions signify areas with substantial structural safety margins. These results affirm that the design remains within safe limits under the specified loading conditions.

Figure 10b further underscores the safety of the optimised design, revealing that the lowest FOS of 2.108 is located at the central loading zone of the crown, where stress peaks; however, this value is still well above the conservative design threshold. Most of the piston volume exhibits FOS values between 5 and 9, particularly in the skirt, pin boss, and side walls, indicating that these areas are structurally underutilised.

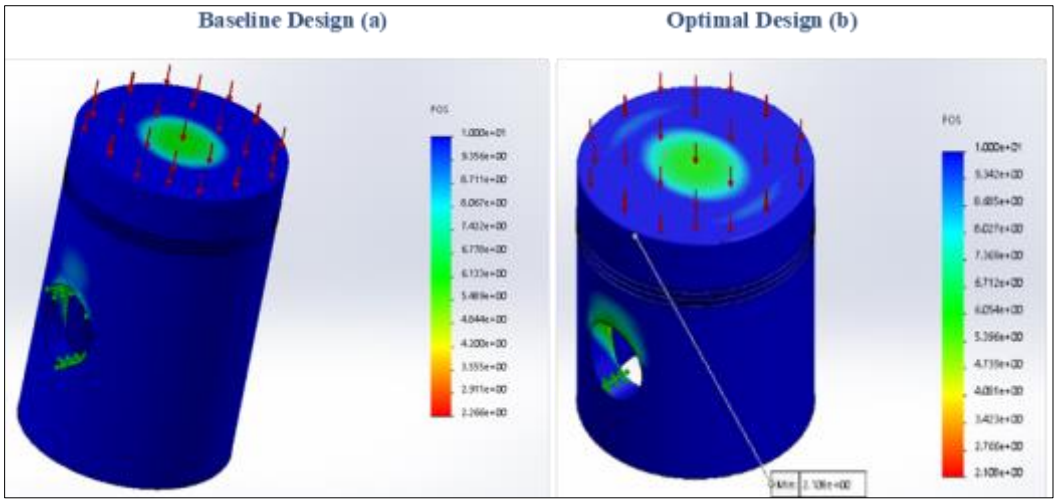

Figure 12 Finite Element Analysis (FEA) visualisation of the Factor of Safety (FOS) Baseline Design (a) and Optimal Design (b) distribution in the piston under applied axial load

As presented in Table 11, the finite element analysis highlighted significant differences in structural performance and weight efficiency among the three piston designs. The baseline design, characterised by a conservative structural approach, exhibited a factor of safety (FOS) of 6.133 and moderate stress levels of 2.738×10^8 N/m^2. However, it also displayed the highest displacement at 0.5238 mm and the heaviest mass at 3594 kg. In contrast, the initial optimal design achieved the lowest displacement of 0.367 mm and reduced the weight by approximately 16.4%, albeit with a slightly diminished safety margin (FOS = 5.440). To assess its robustness, the design was refined and reanalysed. The validated optimal piston maintained satisfactory structural performance, demonstrating a FOS of 6.054 and a moderate displacement of 0.5106 mm, while further reducing weight to 2668 kg, totalling a reduction of over 25.7% compared to the baseline. Although the von Mises stress increased slightly across the optimised models, all values remained well below the material's yield limit, affirming the reliability of the lighter configurations.

Table 11 Comparison of Piston Design Configurations

Design	Height (mm)	Thickness (mm)	Pin dia. (mm)	Material	Displacement (mm)	FOS	Von Mises Stress (N/m^2)	Weight (Kg)
Baseline	1400	120	350	Alloy steel	0.5238	6.133	2.738×10^8	3594
Initial Optimal	1000	120	300	Alloy steel	0.3670	5.440	2.797×10^8	3005
Validated Optimal	1000	120	300	Alloy steel	0.5106	6.054	2.943×10^8	2668

3.3. Comparison with Existing Literature

The optimised piston design was assessed for structural integrity by comparing its von Mises stress levels and factor of safety (FOS) with recent literature on high-load marine engine components. The piston exhibited a maximum von Mises stress of 2.94×10^8 N/m^2 and an FOS of 6.05, which meets or exceeds benchmarks from studies such as those by Kim and Cho (2024), Yang et al. (2023), and Park et al. (2023). Notably, the piston achieved a 25.7% weight reduction without compromising safety, demonstrating improved stress resilience and weight efficiency as shown in Table 12.

Table 12 Evaluation of Piston Stress and FOS with Existing Literature

Study	Component Analysed	Max Stress (N/m^2)	Factor of Safety (FOS)	Remarks
Present Study	Piston (Optimised Design)	2.94×10^8	6.05	25.7% weight reduction; structurally reliable
Kim & Cho (2024).	Marine shafting system	$\leq 3.10 \times 10^8$	5.0 – 6.2	Stress-focused FEA validation under full-load operation
Yang et al. (2023).	Crosshead bearing	$\approx 2.85 \times 10^8$	≥ 5.5	Multi-body tribo-dynamic model under dynamic loading
Park et al. (2023).	Crosshead slipper (engine startup)	$\approx 3.20 \times 10^8$	≥ 5.0	Transient tribo-dynamic FEA under startup stress

4. Conclusion

This study focuses on optimising the structural performance of a two-stroke marine diesel engine piston using parametric modelling, finite element analysis (FEA), and Taguchi-based design of experiments (DOE). Key geometric parameters analysed include piston height, crown thickness, and pin diameter. The optimisation revealed that crown thickness significantly affects the piston's mechanical behaviour, followed by pin diameter and height. The optimise piston, with a height of 1000 mm, crown thickness of 120 mm, and pin diameter of 300 mm, made from alloy steel, achieved a 25.7% weight reduction without sacrificing structural integrity, maintaining a maximum von Mises stress of 2.94×10^8 N/m^2 and a factor of safety of 6.05. The study also confirmed the numerical accuracy of FEA results through grid independence verification. Future research could include thermal cycling, fatigue analysis, and experimental validation to improve the reliability and lifespan of marine diesel pistons.

Compliance with ethical standards

Acknowledgments

The authors express gratitude to the Department of Mechanical Engineering at Niger Delta University for providing access to design and simulation facilities and to the laboratory staff for their technical support. They also appreciate the valuable feedback from colleagues and reviewers, which improved the research.

Disclosure of conflict of interest

No conflict of interest to be disclosed.

References

[1] Chen, M., Zhao, L., & Li, J. (2024). A new tribo-dynamics modelling and online measurement method for marine engines. Ocean Engineering, 293, 116851. https://doi.org/10.1016/j.oceaneng.2024.116851

[2] El-Sayed, A., & Wang, P. (2023). Design and performance evaluation of a low-speed marine diesel engine. Simulation Modelling Practice and Theory, 133, 102803. https://doi.org/10.1016/j.simpat.2023.102803

[3] Kim, T., & Cho, H. (2024). Evaluating the safety of the redesigned shafting system after applying the finite element method. Ocean Engineering, 297, 117023. https://doi.org/10.1016/j.oceaneng.2024.117023

[4] Lin, J., Chen, Y., & Zhou, X. (2022). Measurement of the friction force of sliding friction pairs in low-speed marine diesel engines. Tribology International, 170, 107697. https://doi.org/10.1016/j.triboint.2022.107697

[5] Park, S. H., Lee, J., & Kim, D. (2023). Transient tribo-dynamic analysis of crosshead slipper in low-speed marine diesel engines during engine start-up. Journal of Marine Science and Technology, 28(1), 54–68. https://doi.org/10.1007/s00773-022-00914-1

[6] Uchenna, B. A., & Godwin, O. (2025). Structural modifications for improving the tribological properties of the cylinder unit in two-stroke slow-speed marine diesel engines. IJNAOE, 17(1), 102–114. https://doi.org/10.1016/j.ijnaoe.2024.10.004

[7] Wang, M., Zhu, H., & Yao, Y. (2022). Tribo-dynamic performances and vibration transmission of lubricated crosshead guide joints. International Journal of Mechanical Sciences, 231, 107495. https://doi.org/10.1016/j.ijmecsci.2022.107495

[8] Yang, Q., Wang, Y., & Xu, T. (2023). Crosshead bearing analysis for low-speed marine diesel engines based on a multi-body tribo-dynamic model. Marine Structures, 91, 103299. https://doi.org/10.1016/j.marstruc.2023.103299

[9] Zhang, L., Guo, B., & Li, F. (2025). Stress prediction of marine diesel engine crankshaft based on digital twin technology. Ship Engineering, 47(1), 20–29. https://doi.org/10.19693/j.issn.1673-3185.02833